IOP Publishing Superconductor Science and Technology
Supercond. Sci. Technol. 31 (2018) 125016 (6pp) https://doi.org/10.1088/1361-6668/aae7c2

Change of electronic state in the noncentrosymmetric superconductor Th_7Fe_3

Vinh Hung Tran and Rafał Idczak

Institute of Low Temperature and Structure Research, Polish Academy of Sciences, PO Box 1410, 50-422 Wrocław, Poland

E-mail: V.H.Tran@intibs.pl

Received 7 June 2018, revised 6 October 2018
Accepted for publication 11 October 2018
Published 8 November 2018

Abstract

^{57}Fe Mössbauer spectroscopy and specific heat measurements were performed for the noncentrosymmetric superconductor Th_7Fe_3. An explicit increase in the center shift $\delta_{CS}(T)$, normalised spectral area $A(T)/A(1.5\ \mathrm{K})$ and electric quadrupole splitting $\Delta E_Q(T)$ is observed below $T^* \sim 60$ K. The temperature dependencies of $\delta_{CS}(T)$ and $A(T)/A(1.5\ \mathrm{K})$ follow the Debye model for $T > T^*$, whereas $\Delta E_Q(T)$ can be described by an empirical $T^{3/2}$ equation in both two temperature ranges 2 K–T^* and T^*–300 K. The behaviour of $\Delta E_Q(T)$ can more willingly be interpreted in terms of the Fe^{3+} charge distributions on the singlet (d_{xy}) ground state, the doublet (d_{xz}, d_{zy}) of T_{2g} and doublet ($d_{x^2-y^2}$, d_{x^2}) of E_g excited states, characterised by respective splitting energies Δ_1 and Δ_2. It is shown that the excited energies deduced from the ^{57}Fe Mössbauer data are in good agreement with those of Schottky specific heat. We argue that the anomaly detected in hyperfine parameters and specific heat substantially associates with change in the electronic state of the Fe atoms. We are convinced that a precursor crystal-electric field (CEF) effect has undergone before the onset of superconductivity sets in at lower temperature and the present results would spur new interest to researchers about the interplay between CEF and superconductivity in noncentrosymmetric materials.

Keywords: noncentrosymmetric superconductor, multiple transition, crystal-electric field, Mössbauer spectroscopy

(Some figures may appear in colour only in the online journal)

1. Introduction

Identifying the pairing mechanism responsible for superconductivity is one of the most outstanding challenges for scientists in condensed matter physics. In general terms, the phonon-mediated pairing is the principle mechanism answerable for the isotropic-gap Bardeen–Cooper–Schrieffer (BCS) superconductivity [1]. In contrast, the attractive pairing interaction between electrons in unconventional superconductors (USC) might not be phononic, but presumably associated with the exchange of spin fluctuations [2]. In addition to this issue, there is a need to have complete understanding of how the higher temperature preceding phenomena (e.g., structural distortion, charge-density/spin-density waves or magnetic orderings) affect the lower temperature superconductivity. For this reason, investigations of physical properties of superconductors showing multiple phase transitions are continually desired. Another interesting feature of USC is the possibility of spin-triplet pairing [3]. Anderson suggested many years ago that the center of inversion in the crystal structure is an essential symmetry element for spin-triplet pairing [4]. Thus, the most intriguing case is spin-triplet pairing in the compound $CePt_3Si$ crystallising in a noncentrosymmetric tetragonal structure of the P4mm space group [5]. As a matter of fact, the lack of inversion symmetry creates an electric field gradient (EFG) throughout the system, thus it tallies the presence of antisymmetric spin–orbit coupling (ASOC). This coupling, known as Rashba effect, lifts the electron spin degeneracy of the electronic bands, providing Cooper pairs in NCS to be mixtures of spin-singlet and spin-triplet states [6].

The observation of spin-triplet Cooper pairing in $CePt_3Si$ triggered intensive investigations of many noncentrosymmetric superconductors in the last decade [7]. Keeping in mind the promising effect of noncentrosymmetic structures on superconductivity, we set out to reinvestigate noncentrosymmetric

$Th_7(Fe, Co, Ni)_3$ materials [8–10]. The compounds crystallise in the hexagonal Th_7Fe_3-type structure with the $P6_3mc$ space group [11]. The superconductivity with T_c around 2 K was found by Matthias *et al* [12]. In the meantime, several studies were conducted aiming to determine low-temperature specific heat of these materials. The obtained data have been interpreted in term of the ordinary BCS theory [13–15].

Recently, based on the results of specific heat, electrical resistivity and electronic band structure studies, we confirmed the isotropic-gap superconductivity in Th_7Ni_3 [8], but we suggested an anisotropic superconducting property in Th_7Co_3 [9] and a two-gap superconductivity in Th_7Fe_3 [10]. The difference in the superconducting properties between these superconductors seems to be correlated with splitting energies ΔE_{SO} deduced from the density functional theory calculations. It turns out that the band splitting with a remarkable energy of $\Delta E_{SO} = 100$–120 meV occurs in the exotic Co- and Fe-based superconductors, in contrast to a small energy value of $\Delta E_{SO} = 10$–40 meV found in the ordinary BCS Ni-based one. The presence of ASOC has been apparently seen by an inspection of the splittings of the bands passing the Fermi level (E_F), along the high symmetry line in the first Brillouin zone of hexagonal lattice, i.e., a very pronounced dispersion has been found along Γ–M, A—H, H—K and K–Γ, but a weak split along the A–Γ line. This behaviour is consistent with an anticipated influence of ASOC, which affects perpendicular to those directions where inversion symmetry is missing. For the hexagonal Th_7Fe_3-type structure, the inversion symmetry is broken in the k_z direction (see inset of figure 3).

It is worthwhile to recall that the lattice specific heat $C_{ph}(T)$ of the Th_7Fe_3 compound involving both acoustic and optical phonons would not be applicable to the normal state specific heat below 60 K (see figure 1(a) of [10] and the inset of figure 4). We may add that an application of magnetic fields up to 9 T (not shown here) does not alter the behaviour of the specific heat in this temperature range. Therefore, the low-temperature excess specific heat seems to be not connected to interaction between magnetic moments. In order to shed some light on the specific heat anomaly, and especially to establish the role of EFG in noncentrosymmetric superconductors, we performed Mössbauer spectra measurements for Th_7Fe_3. We will demonstrate that our experimental data not only yield corroborative information about the deviation of phonon properties from the Debye model, but remarkably do provide direct evidence of change in the electronic state of the Fe atoms below 60 K. Furthermore, we strongly propose that a precursor crystal-electric-field effect has undergone before the onset of superconductivity sets in at lower temperature.

2. Experimental details

Two polycrystalline samples of Th_7Fe_3 were synthesised and their quality was checked according to the methods published elsewhere [10]. Sample Th_7Fe_3 marked as No 1 contains 30 at% of the natural iron, while sample $Th_7Fe_{2.5}$ $^{57}Fe_{0.5}$ denoted No 2 possesses 25 at% of the natural iron and 5 at% of the ^{57}Fe isotope (enrichment up to 97.82%). Superconductivity

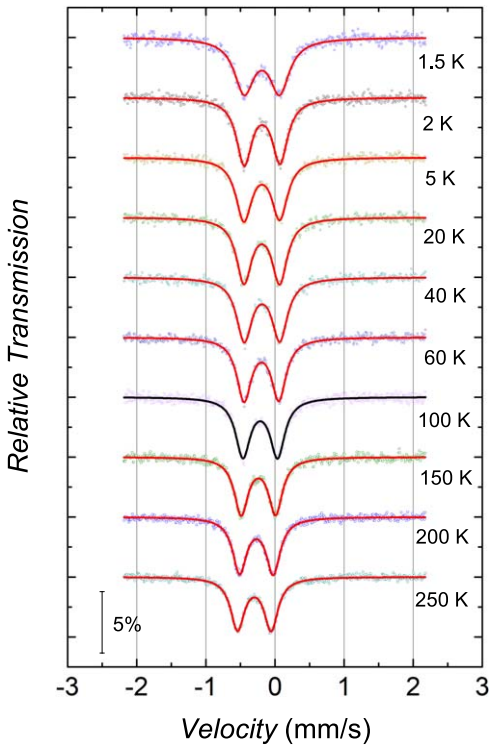

Figure 1. ^{57}Fe Mössbauer spectra of Th_7Fe_3 (sample No 1) in the temperature range 1.5–300 K. The solid lines are theoretical data with the fitting parameters plotted in figures 2 and 3.

with $T_c = 1.98$ K in the studied samples was confirmed by magnetic and specific heat measurement using a Quantum Design MPMS-7XL SQUID magnetometer and 9T-PPMS, respectively. ^{57}Fe Mössbauer spectra were recorded in transmission geometry with a conventional constant acceleration spectrometer. Experimental data were recorded with the help of a 4096-channel analyser. The velocity scale was calibrated with a standard α-Fe foil at room temperature. The powdered samples with surface of 120 mm^2 and thickness of 0.1 mm were placed in thin PVC foils. Sample temperature in the range 1.5–280 K was controlled using a variable-temperature insert in an Oxford Instruments Spectromag cryostat.

3. Results and analysis

Figure 1 presents selected ^{57}Fe Mössbauer spectra of Th_7Fe_3 recorded in the temperature range 1.5–250 K. It is recognized that the data are characterized by well-resolved paramagnetic doublet, implying the presence of electric quadrupole interaction associated with one site of Fe atoms. Obviously, no hyperfine magnetic field was detected in the spectra down to the lowest temperature studied. Nonetheless, the 1.5 K spectrum can be recognised as being broader than the remaining spectra. The effect of the superconducting gap energy on the behaviour of the Mössbauer spectum needs clarification. It is noticed that the Mössbauer spectra collected on sample No 2 in the temperature range 1.5–75 K exhibit very similar characteristic with those of sample No 1. We may

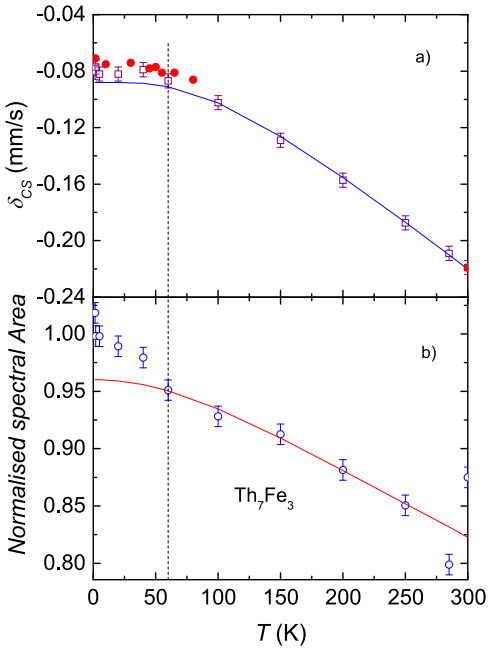

Figure 2. (a) Temperature dependences of the refined center shift δ_{CS} in Th_7Fe_3 (open symbol) and $Th_7Fe_{2.5}$ $^{57}Fe_{0.5}$ (closed symbols). (b) The normalised absorption spectral area under quadrupole doublet $A(T)/A(1.5\,\mathrm{K})$ in Th_7Fe_3 as a function of temperature. The solid lines in (a) and (b) are the results of fitting (see the text). The 300 K data were obtained outside the cryostat.

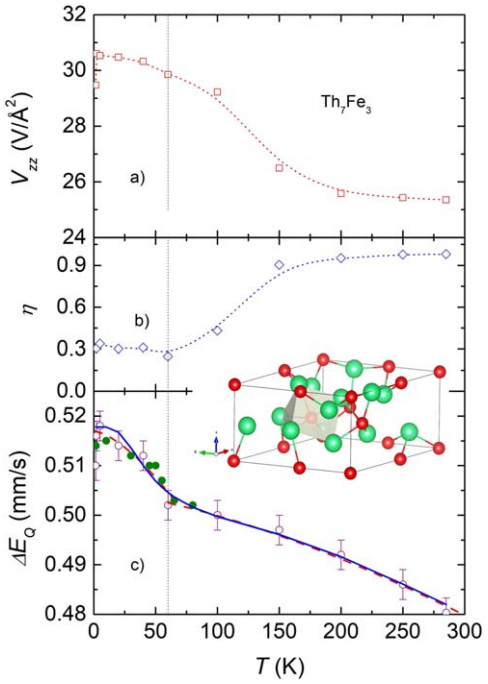

Figure 3. Temperature dependences of (a) the main component V_{zz} of the EFG tensor and (b) asymmetry parameter $\eta(T)$ and (c) quadrupole doublet $\Delta E_Q(T)$. The open symbols are the data of sample No 1 while the closed circles for the sample No 2. The dashed and solid lines are the fits of $\Delta E_Q(T)$ using equations (3) and (4), respectively. Dotted lines in figures (a) and (b) are to guides to the eye. The inset illustrates the crystal structure of Th_7Fe_3.

add that the room temperature spectra (not shown here) coincide well with previously reported data [16].

Taking into account the following hyperfine parameters: electric quadrupole splitting ΔE_Q, center shift δ_{CS} (relative to the isomer shift of metallic Fe), full width at half maximum Γ and spectral area A, we have fitted the experimental data using the MossA fitting software [17]. Satisfactory fits were also obtained if utilizing Moessfit program [18]. In the latter fitting procedure, instead of ΔE_Q we evaluated the principal component V_{zz} of the EFG tensor and asymmetry parameter $\eta = (V_{xx} - V_{yy})/V_{zz}$. The temperature dependences of the refined hyperfine parameters are shown in figures 2 and 3.

Fitting values of the center shift (relative to Fe metal) are found to be negative and lie in the range $-0.22\,\mathrm{mm\,s^{-1}}$ to $-0.08\,\mathrm{mm\,s^{-1}}$. Such a magnitude of δ_{CS} would suggest common states of low-spin configuration, either Fe^{2+} ($S = 0$) or Fe^{3+} ($S = 1/2$) ions [19]. Beware of the paramagnetic Mössbauer quadrupole doublet, which does not support the diamagnetic $S = 0$ configuration, we assume the presence of the paramagnetic $S = 1/2$ state of the Fe^{3+} ions. As shown in figure 2(a), δ_{CS} increases convexly with decreasing temperature, thus the center shift appears to vary with temperature as that expected due to the second-order Doppler effect. Therefore, we have described the temperature dependence of $\delta_{CS}(T)$ using the Debye model [20]:

$$\delta_{CS}(T) = \delta_0 - \frac{3k_BT}{2m_{\mathrm{Fe}}c}\left[\frac{3}{8}\frac{\Theta_D}{T} + 3\left(\frac{\Theta_D}{T}\right)^3\int_0^{\Theta_D/T}\frac{x^3}{e^x - 1}dx\right] \quad (1)$$

where δ_0 is the temperature-independent isomer shift, k_B is the Boltzmann constant, c is the speed of light in vacuum, m_{Fe} is the mass of ^{57}Fe and Θ_D is the Debye temperature. For the data collected in the temperature range 60–300 K, we refined $\delta_0 = 0.016\,\mathrm{mm\,s^{-1}}$ and $\Theta_D = 380\ (\pm 10)$ K.

The temperature dependence of the spectral area of quadrupole doublet, normalised to the value at 1.5 K, $A(T)/A(1.5\,\mathrm{K})$, is shown in figure 2(b). Based on the $A(T)/A(1.5\,\mathrm{K})$ data, we estimated alternatively the Debye temperature using the temperature dependence of the Debye–Waller factor [21] and assuming proportion between the absorption area and the recoilless fraction f [22]. As a result, the theoretical temperature dependence of the normalised absorption spectral area $A(T)/A(1.5\,\mathrm{K})$ is expressed as:

$$A(T)/A(1.5\mathrm{K}) = k\left[\exp\frac{-3E_\gamma^2}{m_{\mathrm{Fe}}c^2k_B\Theta_D}\left(\frac{1}{4} + \left(\frac{T}{\Theta_D}\right)^2\right)\int_0^{\Theta_D/T}\frac{xdx}{e^x - 1}\right], \quad (2)$$

where k is a proportionality constant and $E_\gamma = 14.412\,5$ keV is the energy of the γ ray. Fitting experimental data yields $\Theta_D = 430\ (\pm 20)$ K and recoil free fraction at room temperature $f\,(300\,\mathrm{K}) = 0.79$. The Θ_D value is about 50 K higher than that estimated from the temperature dependence of $\delta_{CS}(T)$. This disagreement may be explained by assumption of different lattice models: the average mean-square displacements of the atoms determine the spectral area while the mean-square velocity ordains the center shift. Nonetheless, an

important message emerges from the fitting data is that the Debye model is able to qualitatively describe the $\delta_{CS}(T)$ and $A(T)/A(1.5\,\mathrm{K})$ in the temperature range 60 K–300 K, thus corroborates what we find in the specific heat experiment. However, there remains a question of interest in our research: what are the possible reasons contributing to an articulate increase in $\delta_{CS}(T)$ and $A(\mathrm{T})/A(1.5\,\mathrm{K})$ at $T^* = 60$ K? First of all, one can take into account a structural phase transition, e.g., distortion from hexagonal to an orthorhombic structure. In principle, a structural change affects the vibrational density of states of the Fe atoms. However, bearing in mind the fact that there is a lack of discontinuous jump in $\delta_{CS}(T)$ and as well as that no anomaly was detected in the electrical resistivity measurement, we are not convinced structural phase transition which would occur. Obviously, persuasive consideration of such a possibility must await low-temperature crystallographic investigations. Let us consider another factor which potentially affects δ_{CS} at T^*. It is generally known that δ_{CS} is in proportion to the electron density at the nucleus as is given by the relation: $\delta_{CS} \propto |\psi_{\mathrm{sample}}(0) - \psi_{\mathrm{source}}(0)|^2$. Therefore, the deviation of $\delta_{CS}(T)$ from the theoretical Debye model curve below T^* simply puts forward a substantial change in the electronic state of the Fe atoms at this temperature. For ^{57}Fe nucleus the moving of δ_{CS} to more positive velocity means a decrease in the s-type electron density. An indirect reason of this feature is related to an increase in the d-type electron density. Because the 3d electrons partly screen the nuclear charge from the 4s electrons, so any gain of the d-type electron density gives rise to better shielding and in a consequence reduces the s-electron density.

The main component $V_{zz}(T)$ of the EFG tensor, asymmetry parameter $\eta(T)$ and the electric quadrupole splitting $\Delta E_Q(T)$ are plotted as a function of temperature in figures 3(a), (b) and (c), respectively. It must be underlined that a reliable upward at 60 K is observed in $V_{zz}(T)$ and $\Delta E_Q(T)$ of both synthesized samples and thus the feature confirms the appearance of thermal anomaly in the Mössbauer hyperfine parameters considered above. Before attempting to analyse the results we may look over the unit cell of Th_7Fe_3 with polyhedron including the central Fe atom (see inset of figure 3). We perceive that the Th atoms occupy three different crystallographic sites with Th_1 at the 2b, Th_2 at 6c and Th_3 at 6c positions, corresponding to 3*m*, *m* and *m* point symmetries, respectively [11]. These positions of those ions in the compound are crystallographically inequivalent and the EFG created by the Th nuclei is conjectured. The Fe atoms at the 6c positions with the *m* point symmetry (see inset of figure 3), having as large as six Th atoms as the nearest neighbours echo the interaction between the quadrupole moment Q of the nuclear excited state the EFG tensor at the Fe site. The resulting quadrupole splitting energy is given by the equation: $\Delta E_Q = \frac{1}{2}eQV_{zz}[1 + \eta^2/3]^{1/2}$, where η is determines the deviation of the EFG tensor from axial symmetry. The fits of the experimental ^{57}Fe Mössbauer data yield a decrease of $\eta(T)$ with decreasing temperature. Such a temperature dependence of $\eta(T)$ suggets a low nonaxial local symmetry at high temperature but a larger symmetry at low temperatures. This feature can be expected in the case of a lack of axial local symmetry at Fe site. Because the proton charge e and the quadrupole moment of the nucleus of ^{57}Fe in the excited state of the Mössbauer transition Q (=0.15 b, [23]) are constant, changes in $\Delta E_Q(T)$ can only arise from changes in the EFG, which basically depend on two factors [20]: (i) the lattice contributions resulting from the charge distribution of the neighbouring ions of Fe nucleus in the lattice and (ii) the valence electron contribution originating from anisotropic distribution of d-electrons in the valence shell. The first contribution is often smaller than the valence one and is temperature independent. The latter factor is temperature dependent and can be evaluated using suitable theoretical models. Similarly as in many non-cubic metals [24], and metallic systems [25], we utilized the empirical equation:

$$\Delta E_Q(T) = \Delta E_Q(0)(1 - BT^{3/2}), \tag{3}$$

where $\Delta E_Q(0)$ is the value of quadrupole splitting at 0 K and B is a constant. The fits of equation (3) to the data give $\Delta E_Q(0) = 0.5175\,\mathrm{mm\,s^{-1}}$ and $B = 5.15 \times 10^{-5}\ \mathrm{K^{-3/2}}$ for the temperature range 2 K–60 K and $\Delta E_Q(0) = 0.5047\,\mathrm{mm\,s^{-1}}$ and $B = 0.95 \times 10^{-5}\ \mathrm{K^{-3/2}}$ for $T = 60$ K–300 K. Unfortunately, the physical meaning of the fitting parameters is less clear.

In preference, we had analysed $\Delta E_Q(T)$ taking into account following effects: the crystal-field splitting, the spin–orbit coupling and co-valency. In a crystal-electric field (CEF) of symmetry lower than tetragonal, the low-spin state of the Fe^{3+} ions has five electrons in the t_{2g} level. Octahedral distortion by ligand fields destabilizes the d_{xz} and d_{yz} orbitals in reference to the orbital d_{xy}. Then the d_{xy} singlet would become the ground state orbital. In the framework of this scheme, we can understand the temperature behaviour of $\eta(T)$ shown in figure 3(b), i.e., the charge distribution is more anisotropic at high temperatures when five electrons are shared between ground state T_{2g} and higher energy E_g orbitals. In contrast, less anisotropy is expected to occur at low temperatures due to localizing two paired electrons on the orbital singlet d_{xy} and three remaining electrons on the first excited state of the doublet d_{xz} and d_{yz}. This physical picture is consistent with calculated values for the quadrupole splitting [19, 20], where the excited states with the hole in a d_{xz} and d_{yz} orbitals yield a positive $\Delta E_Q(T)$. Using the approach developed by Ingalls [26], and Merrithew *et al* [27], we derived the temperature dependence of $\Delta E_Q\ (T)$ for three-level system with Δ_1 and Δ_2 as the splitting energies of the low-energy excited doublet (d_{yz}, d_{xz}) and high-energy excited E_g orbitals from the singlet ground state d_{xy} orbital:

$$\Delta E_Q(T) = \Delta E_Q(0)\left[\frac{(A + a^2e^{-\frac{2\Delta_1}{k_BT}} + b^2e^{-\frac{2\Delta_2}{k_BT}}}{1 + e^{-\frac{\Delta_1}{k_BT}} + e^{-\frac{\Delta_2}{k_BT}}} - \frac{2abe^{-\frac{\Delta_1+\Delta_2}{k_BT})^{\frac{1}{2}}}}{1 + e^{-\frac{\Delta_1}{k_BT}} + e^{-\frac{\Delta_2}{k_BT}}}\right] + \Delta E_{Q,ind}, \tag{4}$$

where A, a and b are parameters accounting for anisotropic orbital mixing and co-valency, $\Delta E_Q(0)$ is the quadrupole splitting at zero temperature and $\Delta E_{Q,ind}$ is the temperature-independent contribution. The best fit yields following values: $\Delta E_Q(0) =$

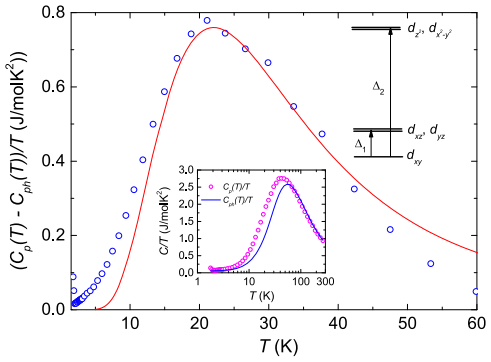

Figure 4. Temperature dependences of difference between the specific heat C_p and phonon contribution C_{ph} divided by temperature. The bottom inset: C_p/T and C_{ph}/T vs T. The upper inset: the crystal-electric-field scheme with the first and second excited states at Δ_1 and Δ_2.

0.4495 mm s^{-1}, $\Delta_1/k_B = 87 \pm 15$ K, $\Delta_2/k_B = 670 \pm 20$ K, $A = 0.476$, $a = -0.7$, $b = -0.2$ and $\Delta E_{Q,ind} = 0.207$ mm s^{-1}. A satisfactory fit (see the solid line in figure 3(c)) implies that $\Delta E_Q(T)$ is strongly influenced by the anisotropic co-valency, spin–orbit coupling and excitation of the charges to the first excited state at the energy Δ_1.

As considered above, there is reason to believe that a sensible interpretation of physical properties can be captured on the basis of the crystal-electric-field effect. So let us go back to the excess specific heat, which is shown in figure 4. In accordance with the scheme of CEF for $\Delta E_Q(T)$, the same three-level system has been applied for the specific heat data. The temperature dependence of the Schottky specific heat $C_{\mathrm{Sch}}(T)$ composed of three different energy levels: the ground state energy level with $\Delta_0 = 0$, the first excited energy level Δ_1 and second excited energy Δ_2, [28] is given:

$$C_{\mathrm{Sch}}(T) = \frac{nR}{T^2}\left[\frac{g_0 g_1(\Delta_1/k_B)^2 e^{-\Delta_1/k_BT} + g_0 g_2(\Delta_2/k_B)^2 e^{-\Delta_2/k_BT}}{(g_0 + g_1 e^{-\Delta_1/k_BT} + g_2 e^{-\Delta_2/k_BT})^2} + \frac{g_1 g_2(\Delta_2/k_B - \Delta_1/k_B)^2 e^{-(\Delta_2+\Delta_1)/k_BT}}{(g_0 + g_1 e^{-\Delta_1/k_BT} + g_2 e^{-\Delta_2/k_BT})^2}\right], \quad (5)$$

where $g_0 = 1$, $g_1 = 2$ and $g_2 = 2$ are the degeneracies of the singlet ground and doublet excited states. R is the gas constant and $n = 3$ for Th_7Fe_3. Using only $\Delta_1/k_B = 75 \pm 15$ K, $\Delta_2/k_B = 650 \pm 20$ K as fitting parameters we obtained the theoretical curve (shown as solid line in figure 4), which satisfactorily reproduces the experimental data points. It is worthwhile to add that CEF effect has been detected in many superconductors. In superconductors such as e.g. $RERh_4B_4$ and $REMo_6S_8$ (RE = rare-earth metal) [29], and $ErNi_2B_2C$ [30], the magnetic interactions between f-electrons are very strong, therefore the influence of CEF on the superconductivity is negligible compared to those of CEF on the ground state splitting. In heavy-fermion superconductors like $PrOs_4Sb_{12}$ [31], UBe_{13} [32], $CeMIn_5$, M = Co, Rh and Ir [33] etc., the CEF may affect the quadrupole fluctuations [34] or orbital fluctuations [35], these further may contribute considerably to superconductivity.

4. Summary

In summary, we have studied the phonon and electronic properties of the noncentrosymmetric superconductor Th_7Fe_3 by Mössbauer spectroscopy. The temperature dependencies of the hyperfine parameters obtained from analysis of the Mössbauer spectra exhibit a distinct increase below 60 K, implying substantial change in the electronic state of the Fe atoms. It was shown that both $\Delta E_Q(T)$ and excess specific heat data can consistently be explained on the basis of same CEF scheme and splitting energies of the same order. Therefore, we believe that CEF effect has to occur before the material undergoes transition into the superconducting state. The observed feature may suggest a crucial role of Coulomb interaction and/or orbital (charge quadrupole) fluctuations in the establishing of a superconducting state. Because, this behaviour is quite unusual among metallic superconductors, we hope very much that the present work will inspire investigations of the interplay between CEF and superconductivity in noncentrosymmetric materials.

Acknowledgment

Financial support by the National Science Centre of Poland under the grant No. 2016/21/B/ST3/01366 is gratefully acknowledged.

ORCID iDs

Vinh Hung Tran https://orcid.org/0000-0001-8811-8991
Rafał Idczak https://orcid.org/0000-0002-4001-8649

References

[1] Bardeen J, Cooper L N and Schrieffer J R 1957 *Phys. Rev.* **106** 162–4
[2] Nakamura S, Moriya T and Ueda K 1996 *J. Phys. Soc. Japan* **65** 4026–33
[3] Ishida K *et al* 2002 *Phys. Rev. Lett.* **89** 037002
[4] Anderson P W 1984 *Phys. Rev.* B **30** 4000–2
[5] Bauer E, Hilscher G, Michor H, Paul C, Scheidt E W, Gribanov A, Seropegin Y, Noël H, Sigrist M and Rogl P 2004 *Phys. Rev. Lett.* **92** 027003
[6] Gor'kov L P and Rashba E I 2001 *Phys. Rev. Lett.* **87** 037004
[7] Smidman M, Salamon M B, Yuan H Q and Agterberg D F 2017 *Rep. Prog. Phys.* **80** 036501
[8] Idczak R, Sahakyan M and Tran V H 2018 *J. Phys.: Condens. Matter* **30** 475802
[9] Sahakyan M and Tran V H 2016 *J. Phys.: Condens. Matter* **28** 205701
[10] Tran V H and Sahakyan M 2017 *Sci. Rep.* **7** 15769
[11] Florio J V, Baenziger N C and Rundle R E 1956 *Acta Crystallogr.* **9** 367–72

[12] Matthias B, Compton V B and Corenzwit E 1961 *J. Phys. Chem. Solids* **19** 130–3
[13] G Sereni J, L Nieva G, G Huber J and E Delong L 1994 *Physica* C **230** 159–62
[14] Pedrazzini P, Schmerber G, Gómez Berisso M, Kappler J and Sereni J 2000 *Physica* C **336** 10–8
[15] Smith J, C Lashley J, M Volz H, Fisher R and Riseborough P 2008 *Phil. Mag.* **88** 2847–50
[16] Viccaro P, Shenoy G, Dunlap B, Westlake D, Malik S and Wallace W 1979 *J. Phys. Colloques* **40** 157–8
[17] Prescher C, McCammon C and Dubrovinsky L 2012 *J. Appl. Crystallogr.* **45** 329–31
[18] Kamusella S and Klauss H H 2016 *Hyperfine Interact.* **237** 82
[19] Gibb T C 10.1007/978-94-009-5923-1 1976 *Principles of Mössbauer Spectroscopy* (New York: Chapman and Hall)
[20] Gütlich P, Bill E and Trautwein A X 2011 *Mössbauer Spectroscopy and Transition Metal Chemistry* (Berlin: Springer)
[21] Boyle A J F and Hall H E 1962 *Rep. Prog. Phys.* **25** 441
[22] Williams J M and Brooks J S 1975 *Nucl. Instrum. Methods* **128** 363–72
[23] Martínez-Pinedo G, Schwerdtfeger P, Caurier E, Langanke K, Nazarewicz W and Söhnel T 2001 *Phys. Rev. Lett.* **87** 062701
[24] Kaufmann E N and Vianden R J 1979 *Rev. Mod. Phys.* **51** 161–214
[25] Albedah M A, Nejadsattari F, Stadnik Z M and Przewoźnik J 2015 *J. Alloys Compd.* **619** 839–45
[26] Ingalls R 1964 *Phys. Rev.* **133** A787–95
[27] Merrithew P B, Rasmussen P G and Vincent D H 1971 *Inorg. Chem.* **10** 1401–6
[28] Tari A 2003 *The Specific Heat of Matter at Low Temperatures* (London: Imperial College Press)
[29] Crow J E, Guertin R P and Mihalisin T W (ed) 1980 Superconductivity *Crystalline Electric Field and Structural Effects in f-Electron Systems* (New York: Plenum Press)
[30] Süllow S, Ludoph B, Snel C E, Kayzel F E, Brück E, Nieuwenhuys G J, Menovsky A A and Mydosh J A 1995 *Z. Phys.* B **98** 17–21
[31] Bauer E D, Frederick N A, Ho P C, Zapf V S and Maple M B 2002 *Phys. Rev.* B **65** 100506
[32] Felten R, Steglich F, Weber G, Rietschel H, Gompf F, Renker B and Beuers J 1986 *Europhys. Lett.* **2** 323
[33] Christianson A D *et al* 2004 *Phys. Rev.* B **70** 134505
[34] Miyake K, Kohno H and Harima H 2003 *J. Phys.: Condens. Matter* **15** L275
[35] Hotta T and Ueda K 2003 *Phys. Rev.* B **67** 104518